

Article

Not peer-reviewed version

Power Systems Frequency Response Enhancement Using Optimal Placement and Sizing of Battery Energy Storage Systems

[Lourence Ngoma](#)*, [Josiah Munda](#), Yskandar Hamam

Posted Date: 27 February 2026

doi: 10.20944/preprints202601.2113.v2

Keywords: battery energy storage systems; frequency nadir; frequency stability; low-inertia power systems; power flow analysis; sensitivity analysis



Preprints.org is a free multidisciplinary platform providing preprint service that is dedicated to making early versions of research outputs permanently available and citable. Preprints posted at Preprints.org appear in Web of Science, Crossref, Google Scholar, Scilit, Europe PMC.

Copyright: This open access article is published under a [Creative Commons CC BY 4.0 license](#), which permit the free download, distribution, and reuse, provided that the author and preprint are cited in any reuse.

Disclaimer/Publisher's Note: The statements, opinions, and data contained in all publications are solely those of the individual author(s) and contributor(s) and not of MDPI and/or the editor(s). MDPI and/or the editor(s) disclaim responsibility for any injury to people or property resulting from any ideas, methods, instructions, or products referred to in the content.

Article

Power Systems Frequency Response Enhancement Using Optimal Placement and Sizing of Battery Energy Storage Systems

Louwrence Ngoma ^{1,*}, Josiah Munda ¹ and Yskandar Hamam ^{1,2}

¹ Department of Electrical Engineering, Tshwane University of Technology, Staatsartillerie Rd, Pretoria 0183, South Africa; mindajl@tut.ac.za

² École Supérieure d'Ingénieurs En Électrotechnique et Électronique, Cité Descartes, Noisy-le-Grand, Paris, France; hamamy@tut.ac.za

* Correspondence: ngomajl@tut.ac.za

Abstract

The increasing penetration of converter-interfaced renewable energy sources has led to a reduction in system inertia and has intensified frequency stability challenges in modern power systems. Battery energy storage systems (BESSs) can provide fast active power support. However, their effectiveness depends on installation location, power rating and network operating conditions. This paper proposes a power flow informed sensitivity based method for the placement and sizing of distributed BESSs to improve frequency nadir performance in low-inertia power systems. The proposed method combines marginal frequency sensitivity obtained from time domain screening simulations with network coupling information derived from power flow. These components are integrated into an optimization formulation subject to practical installation constraints and solved using particle swarm optimization. The method is evaluated using time domain simulations on the IEEE 39-bus New England test system under multiple generator outage contingencies. The results show that BESS locations exhibit non-uniform and nonlinear contributions to frequency nadir and rate of change of frequency improvement. The proposed optimal placement and sizing method distributes BESS capacity across multiple buses based on frequency impact and network coupling. Compared with the baseline case and a benchmark metaheuristic optimal placement and sizing method, the proposed method achieves higher frequency nadirs and lower RoCoF values across all evaluated contingencies. The performance is maintained under load variation scenarios and reduced system inertia due to renewable energy integration. The proposed method provides a physically meaningful and computationally efficient approach for allocating distributed BESSs to support frequency stability in low-inertia power systems.

Keywords: battery energy storage systems; frequency nadir; frequency stability; low-inertia power systems; power flow analysis; sensitivity analysis

1. Introduction

The increasing penetration of converter-interfaced renewable energy sources has led to the gradual displacement of synchronous generators and a corresponding reduction in system rotational inertia. In low-inertia power systems, frequency dynamics following large disturbances become faster, resulting in increased rates of change of frequency (RoCoF) and deeper frequency nadirs after generator outages. These characteristics pose challenges for maintaining frequency stability and secure operation in modern power systems with high shares of non-synchronous generation [1–3].

Battery energy storage systems (BESSs) have been extensively investigated as fast-acting resources for frequency support due to their rapid active-power response and flexible control capabilities. Early studies demonstrated that BESSs can provide effective primary frequency control

and improve frequency nadir performance following large disturbances [4–6]. Subsequent studies showed that BESS-based frequency support can also reduce RoCoF and complement system inertia and conventional reserves in low-inertia power systems [7–10]. These findings collectively establish BESS as a technically viable solution for enhancing initial frequency response following a disturbance.

The effectiveness of BESS placement depends on both location and sizing decisions. Optimization based methods are therefore used to identify suitable locations and power ratings while considering system objectives and operational constraints [11,12]. Sensitivity-based methods have been proposed to provide computationally efficient alternatives for studying the relationship between BESS capacity and frequency response improvement [13]. Time domain simulation studies indicate that increasing BESS capacity enhances frequency nadir and RoCoF performance. However, the incremental enhancement diminishes as BESS sizes increase under severe contingencies [14,15]. This behaviour suggests that effective frequency support cannot be achieved through capacity increase alone and that more informed placement and sizing strategies are required.

The electrical network influences how injected active power propagates through the system. Network topology, impedance distribution and power flow patterns determine the extent to which a local injection contributes to system wide frequency stabilisation. Studies on coordinated control of multiple storage devices indicate that network interactions significantly influence both voltage and frequency behaviour in systems with high renewable penetration [16,17]. Other studies have incorporated impedance based indices and electrical distance metrics into placement formulations [18,19].

Recent optimization strategies have integrated power flow sensitivity information and operating conditions when addressing multiple objectives such as frequency support, voltage regulation and loss minimization. These studies reveal that incorporating power flow related information leads to robust BESS placement and sizing under changing operating conditions [20–22]. However, frequency sensitivity indices derived from dynamic simulations is often treated separately from power flow based metrics. [23,24]. The interaction between frequency response behaviour and the power system network remains insufficiently represented in current BESS placement and sizing methods.

More recent studies have applied optimisation techniques using detailed frequency performance metrics such as nadir, zenith, RoCoF and steady-state frequency [25–27]. while others have considered frequency stability margins and grid operational constraints when determining suitable locations for fast frequency response storage [6,28]. Sensitivity based methods have also been proposed to evaluate the impact of BESS injections across different buses using frequency stability indices such as nadir and RoCoF [29]. In high-renewable systems, hybrid storage placement methods that explicitly consider network constraints have been developed to enhance frequency performance [27].

A structured comparison of representative BESS placement and sizing methods for frequency stability enhancement is provided in Table 1. The comparison highlights differences in the frequency metrics employed, the treatment of network information and the placement and sizing strategies adopted in the literature. The table indicates that most existing methods rely either on frequency response indices or optimization techniques, while explicit integration of power flow informed sensitivity-based placement and sizing methods remains limited.

Table 1. Comparison of BESS placement and sizing methods for frequency stability studies.

Reference	Frequency Metric Used	Network Information	Placement and sizing Strategy
This study	Frequency nadir and RoCoF	Power flow sensitive	Sensitivity + PSO
[25]	Nadir, zenith, RoCoF, steady-state frequency	Frequency dynamics and inertia emulation	GA/PSO optimization

[28]	Frequency stability margin	Grid constraint (frequency regulation)	FFR location optimization
[29]	Frequency nadir and RoCoF	Network effects considered through placement impact across buses	Optimal placement and sizing
[27]	Frequency performance in high-renewable systems	Network constraints within hybrid storage placement method	Hybrid storage placement and sizing

Motivated by the limitations identified in existing studies, this paper proposes a power flow informed sensitivity-based method for optimal placement and sizing of distributed BESSs aimed at improving frequency nadir performance under multiple generator outage contingencies. The proposed method combines marginal frequency sensitivity obtained from time domain screening simulations with network coupling information derived from the Power flow Jacobian. Practical installation constraints, including total BESS capacity and per-bus power limits, are explicitly considered, and the resulting optimization problem is solved using particle swarm optimization. The method is validated using time domain simulations on the IEEE 39-bus test system, and the results demonstrate consistent improvements in frequency nadir and RoCoF compared with baseline operation and a benchmark metaheuristic optimal placement and sizing method.

Unlike existing approaches that use either steady-state electrical distance metrics or dynamic sensitivity indices independently, the proposed method integrates time-domain marginal frequency sensitivity with power flow Jacobian-based network coupling inside a constrained optimisation framework. This enables simultaneous representation of dynamic frequency response effectiveness and steady-state network power transfer capability during candidate bus selection.

The remainder of this paper is organised as follows. Section 2 presents the materials and methods, including the frequency sensitivity formulation and the power flow informed optimization method. Section 3 discusses the simulation results and comparative performance analysis. Section 4 concludes the paper.

2. Materials and Methods

2.1. Study System and Data

The IEEE 39-bus test system is used as the study system to evaluate the proposed battery energy storage system (BESS) placement and sizing method. The system represents a large interconnected transmission network with multiple synchronous generators and load centres and is widely used in frequency stability studies. All dynamic simulations are conducted using DiGSILENT PowerFactory.

Time domain RMS simulations are performed to analyse system frequency response following large generation disturbances. Generator outage events are considered as disturbance scenarios and system frequency signals are recorded at each simulation time step. These signals are used to extract frequency nadir and rate of change of frequency (RoCoF) indices for subsequent analysis using Matlab.

2.2. Frequency Response Modelling

System frequency response is characterised using the system frequency signal obtained from time domain simulations. The baseline frequency nadir for a contingency c , denoted by $f_{nadir,0}^c$, is defined as the minimum frequency value observed following the disturbance in the absence of BESS support. The RoCoF is obtained from the initial slope of the frequency response following the disturbance.

These frequency response indices are used to quantify the severity of each contingency and to evaluate the contribution of BESS injections under different operating conditions. Under-frequency load shedding (UFLS) and protection schemes are not modelled in this study. The objective is to compare the intrinsic electromechanical frequency response under different BESS allocation strategies under identical conditions. The reported frequency nadir values therefore represent

unmitigated system behaviour prior to any UFLS activation. In practical systems, UFLS would likely be triggered at these frequency levels and would influence the subsequent frequency response. Frequency measurements are obtained directly from DIGSILENT PowerFactory dynamic simulations and analysed using a consistent post-processing procedure for all scenarios.

2.3. Sensitivity Based Frequency Screening

To evaluate the impact of BESS placement, dynamic simulations are conducted by placing a single BESS at each bus of the IEEE 39-bus system. Six predefined power ratings (5 MW, 10 MW, 20 MW, 30 MW, 40 MW and 50 MW) are used to evaluate the relationship between BESS size and frequency response. The maximum per-bus BESS size is limited to 50 MW to represent practical installation constraints relative to synchronous generator rating. In the IEEE 39-bus system, where generator ratings range from approximately 300 MVA to 1000 MVA, this corresponds to approximately 5-17% of generator capacity. This ensures that BESS provides fast supplementary frequency support rather than replacing lost generation at a single network location.

For a BESS of size P placed at bus i under contingency c the improvement in frequency nadir is defined as

$$\Delta f_i^{(c)}(P) = f_{i,P}^{(c)} - f_0^{(c)} \quad (1)$$

where $f_{i,P}^{(c)}$ is the resulting frequency nadir.

A linear frequency sensitivity coefficient is obtained using a zero intercept least-square fit, expressed as

$$a_{f,i}^{(c)} = \frac{\sum_p P_p \Delta f_i^{(c)}(P_p)}{\sum_p P_p^2} \quad (2)$$

which represents the marginal frequency nadir improvement per megawatt of BESS power at bus i . An analogous coefficient $a_{f,i}^{(c)}$ is obtained for RoCoF reduction.

Screening results indicate that the incremental frequency benefit of additional BESS power is not strictly linear. To capture this behaviour, a marginal frequency support efficiency is defined as

$$\varepsilon_i^{(c)} = \frac{\Delta f_i^{(c)}(50)}{50 a_{f,i}^{(c)}} \quad (3)$$

which quantifies the extent to which additional BESS power contributes to frequency nadir improvement relative to a linear extrapolation.

2.4. Power Flow Sensitivity Analysis

The effectiveness of BESS power injections is influenced by the electrical characteristics of the transmission network. To capture this effect, power flow sensitivity information is derived from the Power flow solution at the pre-disturbance operating point.

The Newton Raphson Jacobian matrix is used to relate incremental power injections to variations in voltage angles and magnitudes,

$$\begin{bmatrix} \Delta P \\ \Delta Q \end{bmatrix} = \begin{bmatrix} \frac{\partial P}{\partial \theta} & \frac{\partial P}{\partial V} \\ \frac{\partial Q}{\partial \theta} & \frac{\partial Q}{\partial V} \end{bmatrix} \begin{bmatrix} \Delta \theta \\ \Delta V \end{bmatrix} \quad (4)$$

For buses $i \neq j$, with $Y_{ij} = G_{ij} + jB_{ij}$ and $\theta_{ij} = \theta_i - \theta_j$, the Jacobian elements are given by

$$\frac{\partial P_i}{\partial \theta_j} = V_i V_j (G_{ij} \sin \theta_{ij} - B_{ij} \cos \theta_{ij}) \quad (5)$$

$$\frac{\partial P_i}{\partial V_j} = V_i (G_{ij} \cos \theta_{ij} + B_{ij} \sin \theta_{ij}) \quad (6)$$

$$\frac{\partial Q_i}{\partial \theta_j} = -V_i V_j (G_{ij} \cos \theta_{ij} + B_{ij} \sin \theta_{ij}) \quad (7)$$

$$\frac{\partial Q_i}{\partial V_j} = V_i (G_{ij} \sin \theta_{ij} - B_{ij} \cos \theta_{ij}) \quad (8)$$

Considering an active-power-dominant BESS response ($\Delta Q = 0$), the inverse Jacobian is used to evaluate voltage sensitivities to active power injections. The voltage sensitivity of bus m with respect to an active power injection at bus i is defined as

$$S_{V,mi} = \frac{\partial V_m}{\partial P_i} \quad (9)$$

A bus-level network coupling weight is then obtained as

$$\omega_i = \frac{\sum_m |S_{V,mi}|}{\max_j \sum_m |S_{V,mj}|} \quad (10)$$

which represents the relative effectiveness of power transfer from bus i to the network.

The network coupling weight provides a measure of electrical connectivity and active power transfer capability from a given injection location to the broader network and does not directly represent electromechanical frequency dynamics. During transient frequency events, system frequency behaviour is strongly influenced by the manner in which active power imbalance is redistributed across generators and loads through the transmission network. In this context, the network coupling weight acts as a scaling factor that reflects the network-mediated contribution of BESS active power injections to system frequency support.

2.5. Optimization Problem Formulation

The BESS placement and sizing problem is formulated as an optimization problem aimed at improving frequency nadir performance across multiple contingencies. The candidate bus set is obtained from the frequency sensitivity screening described in Section 2.3 and the network electrical effectiveness evaluation described in Section 2.4. The decision variable is the BESS power allocation vector $P = [P_1, P_2, \dots, P_N]$.

For a given BESS allocation, the aggregated marginal frequency efficiency and network effectiveness are defined as

$$\varepsilon^{(c)} = \sum_i \left(\frac{P_i}{P_{tot}} \right) \varepsilon_i^{(c)} \quad (11)$$

$$\omega^{(c)} = \sum_i \left(\frac{P_i}{P_{tot}} \right) \omega_i \quad (12)$$

where P_{tot} is the total installed BESS capacity. The overall effectiveness coefficient is given by

$$k^{(c)} = \varepsilon^{(c)} \omega^{(c)} \quad (13)$$

The expected frequency performance contribution under contingency c is approximated using the combined effectiveness coefficient and the linear frequency sensitivity coefficients obtained from the small-signal screening region: as

$$f_{nadir}^{(c)} = f_0^{(c)} + k^{(c)} \sum a_{f,i}^{(c)} P_i \quad (14)$$

This formulation is applied only during the optimisation search stage to reduce computational burden and provide a computationally efficient surrogate performance indicator for candidate BESS allocation evaluation. The final frequency performance is subsequently verified using full nonlinear time-domain simulations to ensure physical accuracy.

The optimization problem is formulated as

$$\min_P J(P) = \sum_c k^{(c)} \sum a_{f,i}^{(c)} P_i \quad (15)$$

subject to

$$\sum_i P_i = P_{tot}, 0 \leq P_i \leq P_{max} \quad (16)$$

and

$$SoC_{min} \leq SoC_i(t) \leq SoC_{max} \quad (17)$$

The optimization is solved using Particle Swarm Optimization (PSO), which is suitable for the nonlinear and constrained BESS placement and sizing problem. It has been shown to outperform Genetic Algorithms and to achieve superior performance compared with other swarm-based methods such as the Bat Algorithm [25,29]. Each particle represents a candidate BESS allocation vector

$$P_k = [P_{1,k}, P_{2,k}, \dots, P_{N,k}] \quad (18)$$

with velocity vector

$$s_k = [s_{1,k}, s_{2,k}, \dots, s_{N,k}] \quad (19)$$

The velocity and position update equations are

$$s_k(t+1) = \omega s_k(t) + kr_1(t) (P_k^{best} - P_k(t)) + \beta r_2(t) (P_{gbest} - P_k(t)) \quad (20)$$

$$P_k(t+1) = P_k(t) + s_k(t+1) \quad (21)$$

where ω is the inertia weight, k and β are acceleration coefficients, and r_1 and r_2 are random numbers in $[0,1]$. Constraint handling is applied after each update to ensure feasibility. The global best solution obtained from PSO defines the optimal BESS placement and sizing strategy used for final time domain validation.

This sequential screening and optimisation workflow ensures that candidate buses are first filtered based on physical frequency response effectiveness before final sizing optimisation, reducing computational complexity while maintaining physical interpretability.

2.6. BESS and Control Models

The dynamic behaviour of the power system is evaluated using RMS (root mean square) time-domain simulation in DIgSILENT PowerFactory. The RMS simulation framework represents network variables using fundamental-frequency phasor quantities while preserving detailed electromechanical machine dynamics and control system behaviour. This simulation approach is widely used for transient stability and frequency response studies and provides sufficient modelling fidelity for system-level frequency nadir and RoCoF evaluation while enabling efficient multi-contingency analysis.

The synchronous generators are modelled using sixth-order electromechanical synchronous machine models implemented in DIgSILENT PowerFactory. The sixth-order representation includes transient and sub-transient electromagnetic dynamics together with damper winding effects, enabling accurate simulation of fast electromagnetic response and electromechanical oscillation behaviour following disturbances. Each generator model is coupled with excitation system, turbine governor and power system stabiliser models included in the standard IEEE 39-bus dynamic dataset [30].

The battery energy storage system (BESS) is modelled as an inverter-interfaced energy storage unit comprising a frequency controller, a PQ controller, a charge controller, a battery model, and a PWM-based power converter, as illustrated in Figure 1. This configuration enables fast modulation

of active power in response to frequency disturbances while enforcing electrical and energy constraints.

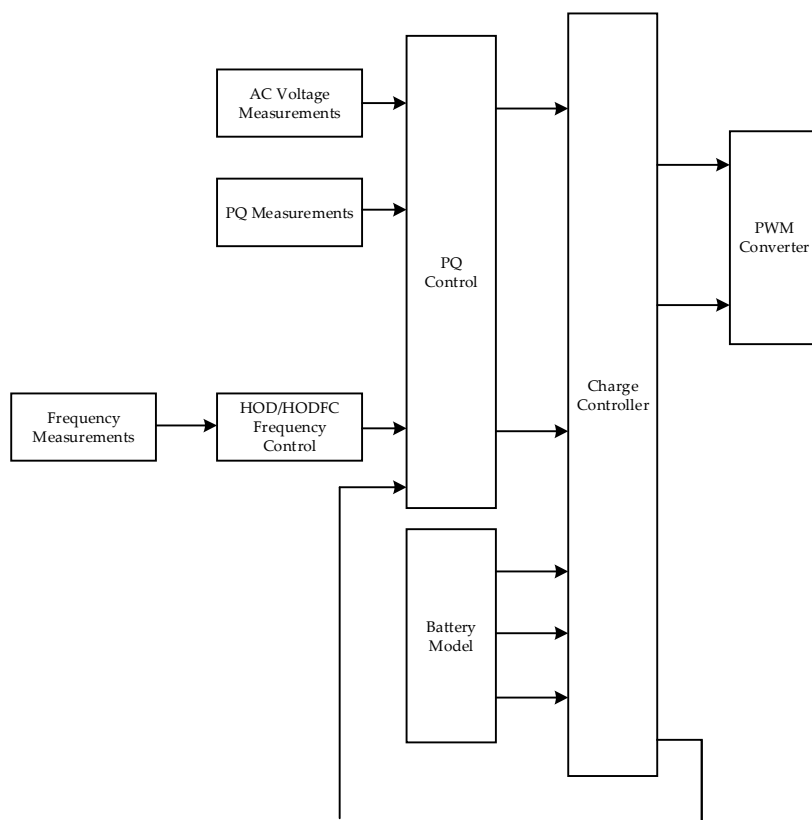


Figure 1. BESS Model.

The BESS receives system frequency, voltage, and power measurements as inputs. Based on these signals, the frequency controller generates an active-power reference command, which is processed by the PQ controller to regulate the active and reactive power exchanged between the BESS and the grid. The charge controller regulates the state of charge (SoC) and power limits using feedback from the battery model. The PWM converter executes the control commands and provides the interface between the BESS and the AC network. Figure 2 presents the frequency control structure implemented in the BESS. The measured system frequency is compared with the nominal reference frequency to generate a frequency deviation signal. A deadband is applied to suppress control action for small frequency deviations. When the frequency deviation exceeds the deadband threshold, a droop-based control law determines the required active-power adjustment. An offset term is included to allow flexible coordination of the BESS operating point.

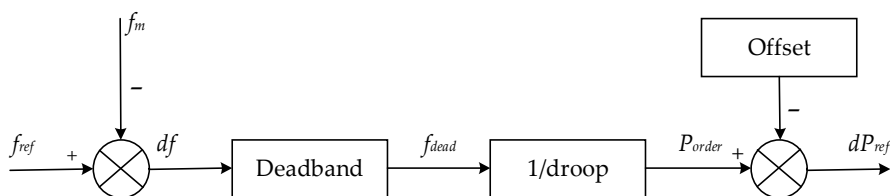


Figure 2. BESS frequency control structure.

The active-power reference generated by the frequency controller is supplied to the PQ controller, which regulates the active and reactive power exchanged between the BESS and the grid using measured voltage and power signals. The PQ controller operates within predefined power limits and ensures stable interaction between the inverter and the network.

To enhance the initial frequency response following disturbances, an inertia emulation control structure is implemented, as illustrated in Figure 3. The controller utilises both system-wide and local frequency dynamics to determine the required fast active power injection.

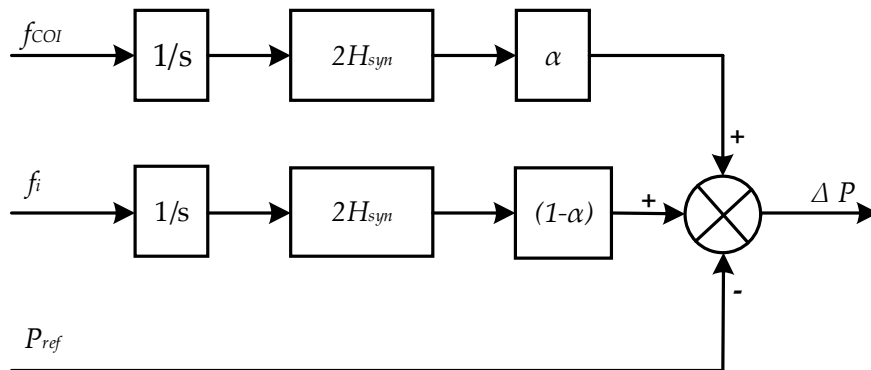


Figure 3. BESS inertia emulation control.

The centre-of-inertia (COI) frequency represents the inertia-weighted average frequency of all synchronous generators and is defined as

$$f_{COI}(t) = \frac{\sum_{i=1}^N S_i H_i f_i(t)}{\sum_{i=1}^N S_i H_i} \quad (22)$$

where H_i is the inertia constant of generator i , S_i is the rated apparent power, and $f_i(t)$ is the generator electrical frequency.

The COI rate of change of frequency is given by

$$RoCoF_{COI}(t) = \frac{df_{COI}(t)}{dt} \quad (23)$$

In addition to system-level frequency dynamics, local bus frequency behaviour is represented using local RoCoF

$$RoCoF_i(t) = \frac{df_i(t)}{dt} \quad (24)$$

From power system dynamics theory, RoCoF is directly related to system inertia and active power imbalance. Based on the swing equation

$$\frac{df}{dt} = \frac{f_0}{2H_{sys}} \Delta P \quad (25)$$

where f_0 is the nominal frequency, H_{sys} is the equivalent system inertia and ΔP is the generation to load power imbalance. This relationship indicates that fast active power injection from BESS units directly reduces RoCoF magnitude by compensating for the active power imbalance during the initial disturbance period.

An inertia emulation control structure is implemented to provide fast frequency support during the initial disturbance period, as shown in Figure 3. The COI frequency f_{COI} and the local bus frequency f_i are independently differentiated to obtain their respective RoCoF signals. Each RoCoF signal is scaled by the same synthetic inertia gain $2H_{syn}$. The resulting inertia contributions are weighted using a factor α , such that the COI-based component is scaled by α and the local bus-based component is scaled by $(1 - \alpha)$.

The combined inertia-based active power contribution is expressed as

$$\Delta P_i(t) = 2H_{syn}[\alpha RoCoF_{COI}(t) + (1 - \alpha)RoCoF_i(t)] \quad (26)$$

where $0 \leq \alpha \leq 1$ controls the relative contribution of global and local frequency dynamics. The inertia-based power contribution is superimposed on the steady-state active power reference P_{ref} to generate the final active power command supplied to the PQ controller.

The BESS frequency support controller operates as a fast outer-loop supplementary control layer that enhances system frequency response without modifying the internal control loops of synchronous generators. From a small-signal perspective, the inertia emulation controller introduces an additional fast active power feedback path proportional to measured frequency dynamics. For moderate values of H_{syn} , this behaviour contributes additional effective damping to the electromechanical frequency response. Excessive values of H_{syn} may introduce phase lag between frequency measurement and active power injection, which may reduce damping and potentially introduce oscillatory behaviour. The selected controller parameter ranges were verified using nonlinear time-domain simulations to ensure stable frequency recovery behaviour across all investigated contingencies.

The interaction between global COI frequency dynamics and local RoCoF measurements is influenced by network coupling strength. Local RoCoF signals may contain higher-frequency components associated with local generator oscillations or weakly coupled network areas. Excessive weighting of local RoCoF signals may increase sensitivity to local oscillatory modes. The blending factor α is selected to maintain dominant contribution from global frequency dynamics while preserving local disturbance sensitivity.

The BESS converter, battery energy storage, and frequency controller parameters used in this study are based on standard inverter-based energy storage control structures available in DIGSILENT PowerFactory. The selected parameter values represent fast active power response relative to synchronous generator mechanical response dynamics and are suitable for grid frequency support applications. The detailed numerical values of converter control parameters, battery energy constraints, and frequency controller settings are provided in Appendix A (Tables A1–A3).

The BESS controller, battery energy model, and optimization framework are implemented using fixed parameter values applied consistently across all simulation scenarios. This ensures consistent evaluation of BESS frequency support performance across multiple contingencies, load levels, and system inertia conditions.

3. Results

3.1. Test System Description

The IEEE 39-bus New England test system is employed to evaluate the proposed BESS placement and sizing strategy using DIGSILENT PowerFactory, which enables detailed electromechanical modelling of synchronous generators, network components, and system frequency dynamics. The system represents a realistic large-scale transmission network derived from the New England power system and consists of multiple synchronous generators with non-uniform ratings and inertia constants interconnected through a meshed transmission network, as illustrated in Figure 4.

The generator ratings and inertia constants implemented in the DIGSILENT model are summarised in Table 2, resulting in a non-uniform inertia distribution across the network. This spatial variation in inertia plays a key role in shaping system frequency behaviour following disturbances and provides a suitable basis for assessing network-aware frequency support strategies.

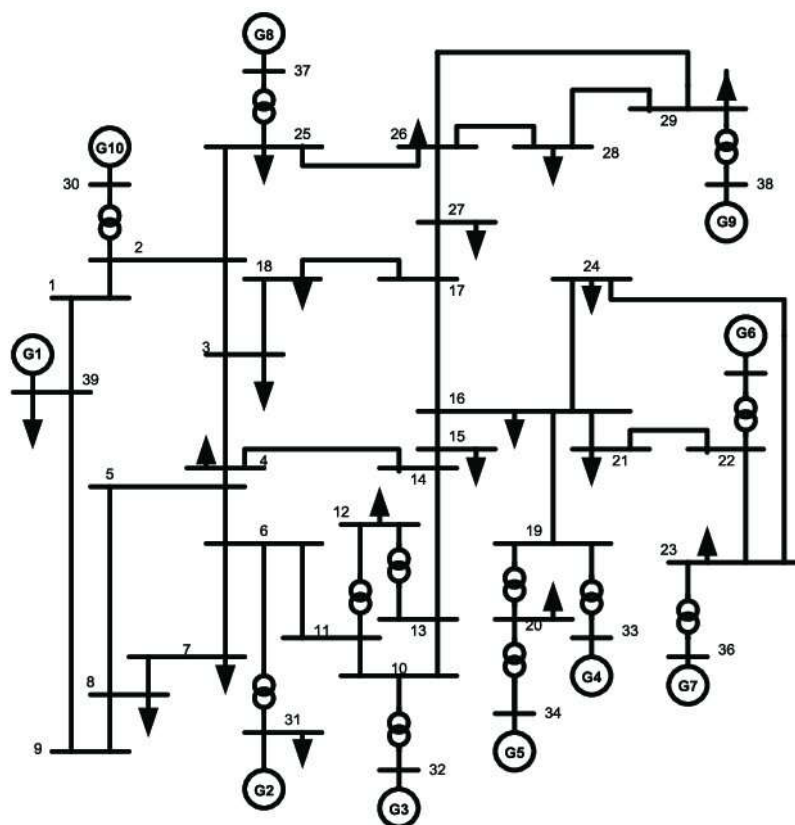


Figure 4. IEEE 39 bus New England system.

Table 2. Generator ratings and inertia constants of the IEEE 39-bus New England test system.

Generator	Bus No.	Rated Apparent Power (MVA)	Inertia, H (s)
G1	30	1000	5.00
G2	31	700	4.33
G3	32	800	4.48
G4	33	800	3.58
G5	34	300	4.33
G6	35	800	4.35
G7	36	700	3.77
G8	37	700	3.47
G9	38	1000	3.45
G10	39	1000	4.00

System frequency performance is evaluated under a set of credible generator outage contingencies, corresponding to the disconnection of generators G01, G03, and G09, which represent disturbances of varying severity. These contingencies are applied consistently across all analysed cases to ensure a fair and systematic comparison between the baseline configuration, the metaheuristic-based placement and sizing method, and the proposed power flow informed sensitivity-based method. All contingencies are simulated as sudden generation losses at the nominal operating point, and the resulting frequency nadir and RoCoF responses are extracted from the DIgSILENT simulations for subsequent analysis.

3.2. Baseline Frequency Response without BESS

The baseline system frequency response is evaluated under generator outage contingencies corresponding to G01, G03, G04, G06, and G09 without BESS support. These contingencies represent

disturbances with different severity levels and electrical coupling characteristics within the network. The resulting frequency nadir and RoCoF values are summarised in Table 3, while the corresponding frequency responses are presented in Figure 5. The reported frequency values represent the intrinsic electromechanical system response because under-frequency load shedding (UFLS) and protection schemes are not modelled. In practical power systems, UFLS would likely activate at these frequency levels, which would influence the subsequent frequency recovery behaviour.

The G01 outage produces the most severe frequency response. The minimum frequency nadir reaches 55.923 Hz while the RoCoF reaches approximately 0.24006 Hz/s. This behaviour reflects a large instantaneous power imbalance combined with strong electrical coupling of the generator to the network. The rapid frequency decline indicates high system sensitivity to the loss of this unit.

The G09 outage produces a less severe response compared with G01. The frequency nadir reaches approximately 56.843 Hz while the RoCoF reduces to approximately 0.10396 Hz/s. The improved performance relative to G01 is associated with reduced effective inertia loss or lower electrical influence of the disconnected generator.

Moderate contingencies such as G04 and G06 produce higher frequency nadirs with lower RoCoF values. The G04 outage results in a frequency nadir of approximately 57.839 Hz with RoCoF of approximately 0.07412 Hz/s. The G06 outage produces a frequency nadir of approximately 57.923 Hz with RoCoF of approximately 0.07267 Hz/s. These responses indicate lower disturbance severity compared with major generator outages.

The G03 contingency produces one of the highest nadir values among the evaluated cases. The frequency nadir reaches approximately 57.958 Hz while RoCoF remains close to 0.07254 Hz/s. This response indicates reduced disturbance propagation through the network compared with strongly coupled generator outages.

The baseline results establish a reference case for evaluating BESS-based frequency support strategies under identical disturbance conditions.

Table 3. Baseline frequency stability indices.

Generator	Nadir (Hz)	RoCoF (Hz/s)
G01	55.923	0.24006
G09	56.843	0.10396
G04	57.839	0.074123
G06	57.923	0.072668
G03	57.958	0.072543

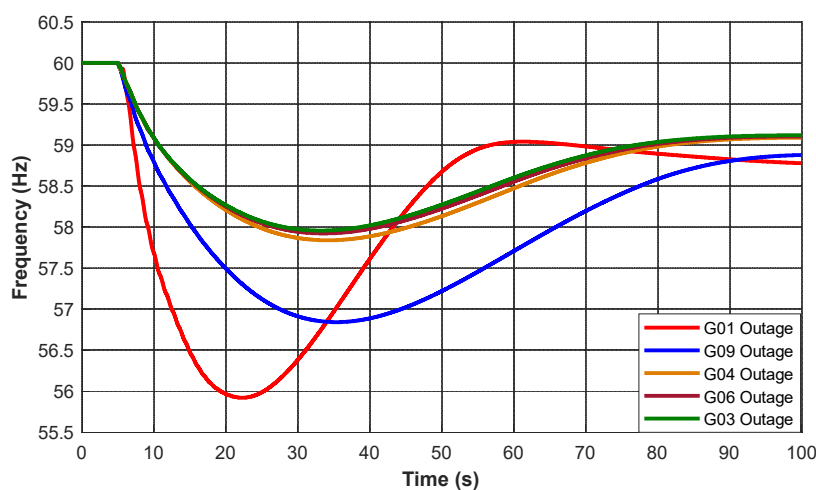


Figure 5. Baseline system frequency response.

3.3. Frequency Contribution of BESS Locations

This section evaluates the contribution of BESS power capacity to system frequency performance while maintaining a fixed installation location plus control structure. The analysis considers BESS capacities of 0 MW, 5 MW, 10 MW, 20 MW, 30 MW, 40 MW, 50 MW, which represent the practical installation range evaluated during screening simulations. The objective is to isolate the influence of BESS size on frequency nadir improvement as well as RoCoF reduction. The simulation results are summarised in Table 4 while the corresponding frequency nadir improvement behaviour is presented in Figure 6.

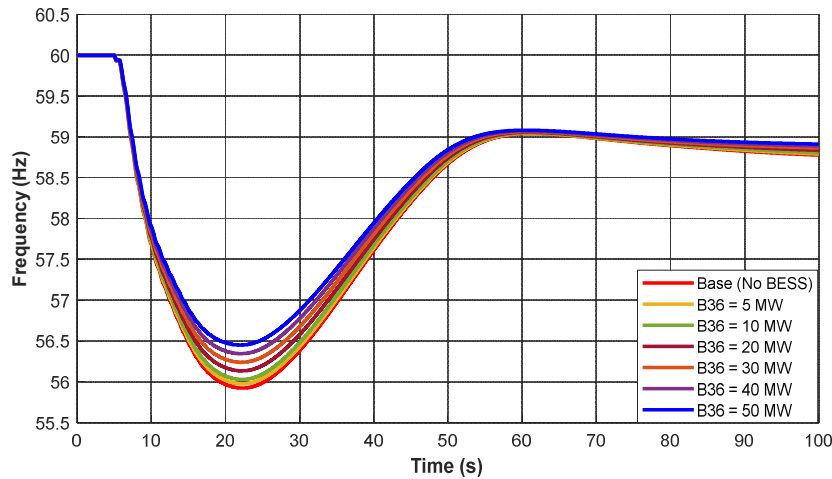


Figure 6. BESS size and frequency nadir improvement.

For the baseline case without BESS, the frequency nadir is 55.923 Hz while RoCoF is 0.24006 Hz/s. The addition of a 5 MW BESS increases the frequency nadir to 55.976 Hz while reducing RoCoF to 0.23654 Hz/s. Increasing BESS capacity to 10 MW increases the frequency nadir to 56.028 Hz while RoCoF reduces to 0.23401 Hz/s. These results confirm that even small BESS installations provide measurable frequency support during the initial disturbance period.

Increasing BESS capacity further improves frequency performance. At 20 MW, the frequency nadir reaches 56.134 Hz while RoCoF reduces to 0.22741 Hz/s. At 30 MW, the frequency nadir increases to 56.239 Hz while RoCoF reduces to 0.22163 Hz/s. At 50 MW, the frequency nadir reaches 56.449 Hz while RoCoF reduces to 0.20923 Hz/s. These values represent the maximum improvement relative to the baseline case within the investigated capacity range.

Table 4. Frequency response versus BESS size.

BESS Size (MW)	f_{nadir} (Hz)	RoCoF (Hz/s)
0	55.923	0.24006
5	55.976	0.23654
10	56.028	0.23401
20	56.134	0.22741
30	56.239	0.22163
40	56.344	0.21529
50	56.449	0.20923

Figure 6 illustrates that frequency nadir improvement is approximately linear at lower BESS capacities. Nonlinear behaviour becomes more pronounced as BESS capacity increases. Increasing BESS capacity from 10 MW to 30 MW improves the frequency nadir by approximately 0.211 Hz. Increasing capacity from 30 MW to 50 MW produces a similar improvement of approximately 0.210

Hz despite identical capacity increase. This behaviour indicates diminishing marginal frequency contribution at higher BESS capacities.

The nonlinear response is associated with system dynamic constraints during the transient frequency response period. At higher BESS power levels, incremental active power injection effectiveness is limited by network power transfer capability, generator electromechanical response limits, plus system damping characteristics.

These results confirm that increasing BESS capacity alone does not guarantee proportional frequency performance improvement. Coordinated BESS placement plus sizing is required for effective utilisation of installed storage capacity. This observation motivates the combined sensitivity-based plus network-aware placement formulation introduced in the following sections.

3.4. Network Influence Based on Power flow Information

The effect of network power flow characteristics on the performance of BESS based frequency support is examined using the proposed sensitivity-based network indices. The relationship between the derived network influence weights and the corresponding behaviour of the frequency response is illustrated in Figure 7 and summarised in Table 5.

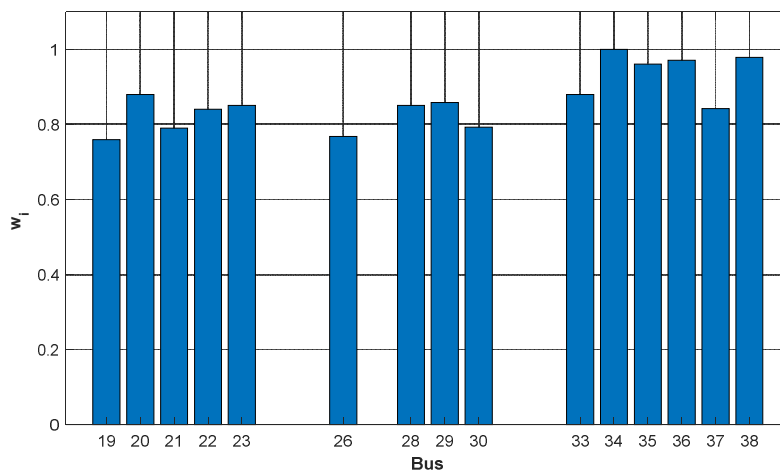


Figure 7. Network influence weights.

Table 5 shows a clear variation in the weighting factors ω_i across the IEEE 39-bus system. The highest values are observed at buses 34, 38, 36, and 35. All these buses exceed 0.96 which shows strong electrical coupling with the rest of the network. By contrast, buses such as 31, 6, and 5 exhibit substantially lower weights reflecting weaker coupling to dominant power flow paths.

Table 5. Weighting factors ω_i for the IEEE 39-bus system.

Rank	Bus	ω_i	Rank	Bus	ω_i	Rank	Bus	ω_i
1	34	1.00000	14	26	0.76787	27	32	0.59839
2	38	0.97845	15	19	0.75934	28	12	0.56679
3	36	0.97138	16	24	0.75479	29	9	0.55314
4	35	0.96105	17	27	0.75206	30	14	0.51229
5	20	0.87967	18	25	0.72151	31	13	0.50484
6	33	0.87967	19	16	0.69917	32	10	0.47806
7	29	0.85812	20	17	0.69679	33	4	0.47681
8	23	0.85105	21	1	0.68428	34	8	0.43631
9	28	0.85085	22	2	0.67263	35	11	0.42354
10	37	0.84184	23	18	0.66361	36	7	0.41915
11	22	0.84072	24	39	0.63658	37	5	0.37237

12	30	0.79296	25	3	0.62195	38	6	0.32033
13	21	0.79058	26	15	0.61733	39	31	0.20000

Buses associated with higher network influence weights provide stronger mitigation of frequency deviations when the same BESS capacity is applied. This behaviour is linked to the way transient active power injections propagate through the grid. Electrically well coupled locations allow injected power to reach a broader portion of the system more effectively which improves the system level frequency response.

These results show that the impact of BESS placement is not uniform across candidate buses. The electrical position of the location within the grid plays an important role in determining the effectiveness of frequency support. Accounting for network influence is therefore necessary when selecting suitable locations for BESS deployment.

3.5. Frequency Sensitivity Index Distribution

This section evaluates the distribution of marginal frequency sensitivity across the IEEE 39-bus system using the normalised frequency sensitivity coefficient. The ranking is presented in Table 6 and the corresponding distribution is shown in Figure 8. The frequency sensitivity coefficient represents the marginal improvement in frequency nadir per unit BESS power injection obtained from time-domain screening simulations.

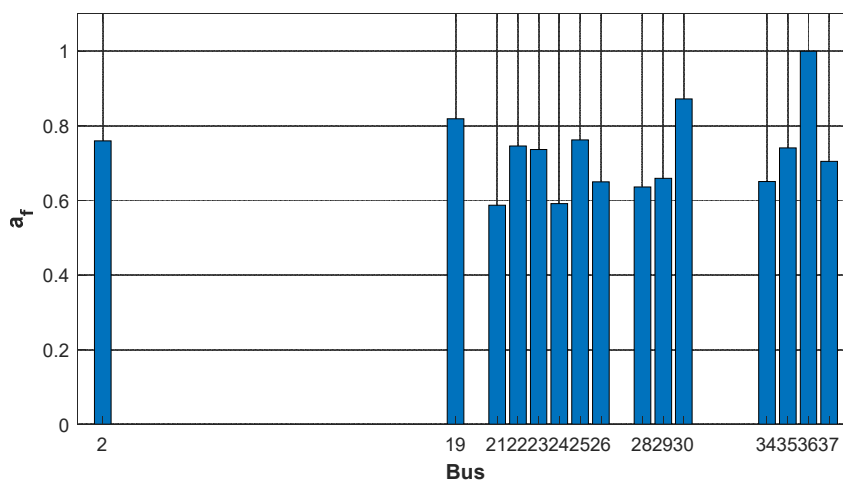


Figure 8. Frequency sensitivity ranking.

Table 6. Frequency sensitivity ranking for the IEEE 39-bus system.

Rank	Bus	a_f
1	36	1.00000
2	30	0.87177
3	19	0.81885
4	25	0.76212
5	2	0.75978
6	22	0.74557
7	35	0.74085
8	23	0.73625
9	37	0.70456
10	29	0.65935
11	34	0.65082
12	26	0.64975
13	28	0.63631

14	24	0.59119
15	21	0.58670
16	38	0.57132
17	16	0.55734
18	33	0.55728
19	1	0.54662
20	17	0.54534

Frequency sensitivity is non-uniform across the network. Bus 36 exhibits the highest normalised sensitivity value of 1.000, indicating the strongest marginal frequency nadir improvement per megawatt of BESS power injection. Bus 30 and Bus 19 follow with values of 0.87177 and 0.81885, respectively. Other high-ranking buses include Buses 25, 2, 22, 35, and 23, all with normalised sensitivity values above approximately 0.73. These buses provide stronger dynamic frequency support relative to lower-ranked locations. Mid-ranked buses such as 34, 26, 28, and 24 show sensitivity values between approximately 0.59 and 0.65. Lower-ranked buses exhibit values close to 0.54, indicating reduced marginal frequency contribution. The distribution shown in Figure 8 indicates that dominant marginal frequency improvement is concentrated in a limited number of buses.

Frequency response effectiveness is strongly dependent on BESS installation location. Frequency sensitivity alone does not represent system-wide effectiveness. The sensitivity index is therefore combined with network influence information in the impact index formulation presented in Section 3.6.

3.5.1. Cross-Scenario Validation of Frequency Sensitivity Ranking

The sensitivity ranking is evaluated across multiple operating scenarios including contingency variation, load variation, and reduced inertia conditions. The cross-scenario comparison is presented in Table 7.

Table 7. Frequency sensitivity ranking.

Scenario	G01 Outage		G09 Outage		G01 Outage + 10% Load Increase		G01 Outage + G08 Replaced with Renewable Generation	
	Rank	Bus a_f	Bus	a_f	Bus	a_f	Bus	a_f
1	36	1.00000	36	1.00000	36	1.00000	36	1.00000
2	35	0.97246	35	0.91982	19	0.92835	30	0.91496
3	22	0.91764	22	0.83408	30	0.86150	29	0.81991
4	30	0.91299	19	0.79888	22	0.85303	2	0.78415
5	19	0.89945	30	0.79764	35	0.82344	25	0.78317
6	23	0.89479	23	0.78833	23	0.81366	28	0.76142
7	29	0.88016	2	0.71769	29	0.81184	19	0.75363
8	28	0.85795	37	0.67872	28	0.78206	38	0.69253
9	38	0.85479	25	0.66913	25	0.77639	26	0.65883
10	37	0.83154	21	0.62350	2	0.76903	1	0.63137
11	34	0.82839	34	0.61888	38	0.73796	37	0.62111
12	25	0.81978	1	0.59171	26	0.73198	34	0.48803
13	26	0.81358	24	0.58911	37	0.68688	23	0.44824
14	21	0.81023	16	0.54567	21	0.67049	27	0.42715
15	33	0.78638	33	0.52329	34	0.66799	3	0.41111
16	24	0.78614	3	0.50189	1	0.66357	22	0.37751
17	2	0.76827	10	0.49156	24	0.64224	17	0.36260
18	16	0.76400	17	0.48395	27	0.61808	10	0.35925
19	27	0.75329	18	0.47380	16	0.60369	18	0.35544
20	17	0.74131	13	0.46044	17	0.59351	16	0.35435

Bus 36 remains ranked first across all evaluated scenarios. Under nominal contingency conditions (G01 and G09 outages), Buses 35, 22, 30, 19, and 23 remain within the highest-ranking group, with minor ordering differences between contingencies. Under increased loading conditions, the same candidate bus group remains dominant, with ranking variation mainly observed in mid-ranked buses.

Under reduced inertia conditions, Bus 36 and Bus 30 remain among the highest ranked locations. Buses such as 29, 2, 25, and 28 increase in ranking, indicating increased importance of electrically well-coupled buses under low inertia operation.

The cross-scenario results confirm that the dominant frequency sensitivity buses remain consistent across contingency variation, loading changes, and reduced inertia conditions.

3.6. Combined Network-Aware Effectiveness

The combined influence of frequency response sensitivities and network characteristics is assessed using the proposed impact index which integrates both dynamic response and power flow information. The ranking of candidate buses based on this index is illustrated in Figure 9 and the corresponding numerical values are reported in Table 8.

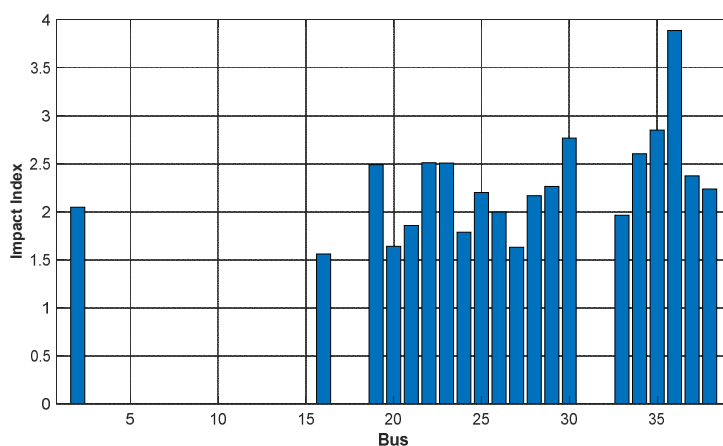


Figure 9. Ranking of candidate buses according to the frequency impact index.

Table 8. Ranked Impact Index values for all candidate buses.

Rank	Bus	Impact Index
1	36	3.8855
2	35	2.8480
3	30	2.7651
4	34	2.6033
5	22	2.5072
6	23	2.5064
7	19	2.4871
8	37	2.3725
9	29	2.2632
10	38	2.2360
11	25	2.1995
12	28	2.1656
13	2	2.0442
14	26	1.9957
15	33	1.9609
16	21	1.8553
17	24	1.7849

18	20	1.6398
19	27	1.6296
20	16	1.5587

As shown in Table 8, buses 36, 35, and 30 achieve the highest impact index values, indicating that these locations provide the most favourable balance between frequency response effectiveness and network influence. Bus 36 is ranked first with an impact index of 3.8855, followed by buses 35 and 30 with values of 2.8480 and 2.7651, respectively. At the other end of the ranking, buses such as 27 and 16 show noticeably lower index values, indicating reduced suitability for effective frequency support under the same BESS capacity.

The ranking presented in Figure 9 highlights that candidate buses are not uniformly suitable for BESS placement. Locations that perform well in terms of marginal frequency sensitivity alone do not always achieve the highest combined effectiveness once network characteristics are considered. The impact index therefore provides a more balanced measure for identifying candidate buses that are both dynamically effective and electrically well positioned.

3.7. Optimized BESS Placement and Sizing

The BESS placement and sizing problem is solved using Particle Swarm Optimization (PSO) with a constrained total BESS capacity of up to 300 MW. The per-bus power is limited to 50 MW, and the number of installation buses is also constrained. The resulting allocation is summarised in Table 9.

Table 9. Optimized BESS placement and sizing.

Bus	Voltage (kV)	BESS Size (MW)
36	16.5	46
35	16.5	34
30	16.5	32
34	16.5	30
22	345	29
23	345	29
19	345	29
37	16.5	28
29	345	26

The optimized solution distributes the available BESS capacity across multiple buses instead of allocating the maximum capacity to a single location. As shown in Table 9, the highest allocation is assigned to bus 36 with 46 MW. This is followed by bus 35 with 34 MW and bus 30 with 32 MW. Moderate allocations are assigned to buses 34 with 30 MW, 22 with 29 MW, 23 with 29 MW, and 19 with 29 MW. Smaller allocations are assigned to buses 37 with 28 MW and 29 with 26 MW.

The allocation trend reflects the combined influence of electrical coupling and frequency response effectiveness. Buses with larger BESS sizes correspond to locations where injected active power produces higher frequency nadir and reduced RoCoF. This enables more efficient use of the constrained storage resource. Smaller allocations indicate locations where system frequency is less sensitive to power injection, resulting in reduced contribution to frequency nadir and RoCoF improvement.

Figure 10 shows the evolution of the objective function value across PSO iterations for the constrained BESS placement and sizing problem. The objective function decreases rapidly during the early iterations demonstrating effective exploration of the search space. As the iterations progress the rate of improvement decreases and the curve stabilises. The stabilisation of the objective function after convergence indicates that the algorithm does not exhibit significant oscillations or instability in the later stages of the optimization process. This behaviour reflects a suitable balance between

exploration and exploitation within the PSO search mechanism. The convergence pattern observed in Figure 10 demonstrates that PSO is capable of efficiently navigating the solution space and producing a stable final solution for the constrained BESS allocation problem considered in this study.

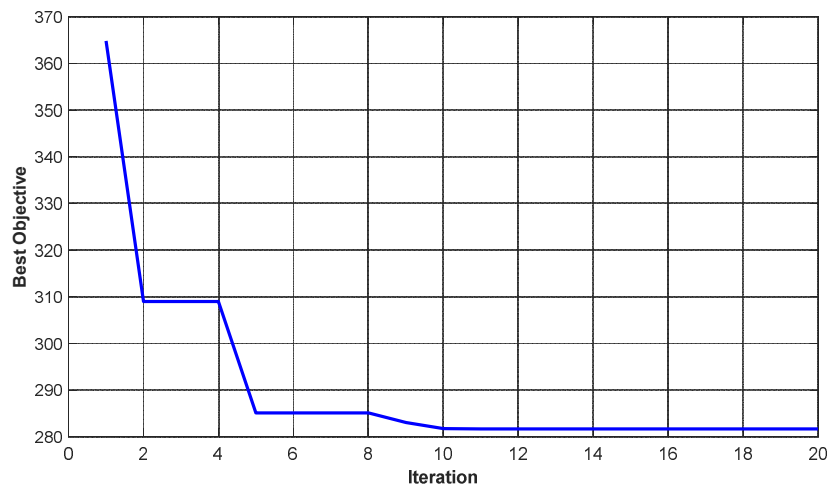


Figure 10. PSO convergence.

3.8. BESS Placement and Sizing Obtained Using PSO

The frequency response of the IEEE 39-bus New England system with the optimized BESS allocation is evaluated using time domain simulations in DIgSILENT PowerFactory. A comparison between the baseline case (without BESS), the metaheuristic-based method [29] and the proposed method is reported in Table 10 for the selected contingencies (G01, G09, and G03).

Table 10. Frequency stability comparison.

Method	G01 Outage		G09 Outage		G03 Outage	
	f_{nadir} (Hz)	RoCoF (Hz/s)	f_{nadir} (Hz)	RoCoF (Hz/s)	f_{nadir} (Hz)	RoCoF (Hz/s)
Proposed Method	58.6561	0.1224	58.7552	0.0519	59.3854	0.0333
Metaheuristic	58.4690	0.1365	58.5881	0.0576	59.2927	0.0401
Without BESS	55.9230	0.2404	56.8434	0.1040	57.9577	0.0725

Across all contingencies, the proposed method achieves the highest frequency nadirs and the lowest RoCoF values. For the most severe disturbance (G01 outage), the frequency nadir increases from 55.9230 Hz in the baseline case to 58.6561 Hz with the proposed method, corresponding to an improvement of 2.7331 Hz (4.88%), while RoCoF decreases from 0.2404 Hz/s to 0.1224 Hz/s. The metaheuristic method achieves intermediate performance with a nadir of 58.4690 Hz and a RoCoF of 0.1365 Hz/s. Similar trends are observed for the G09 and G03 outages where the proposed method consistently delivers superior frequency performance.

Figure 11 presents the frequency response for the G01 outage. The proposed method exhibits a flatter initial decline and smoother recovery than both the baseline and the metaheuristic method. This indicates stronger containment of the disturbance and improved damping during the critical post-fault interval. Figure 12 shows the response for the G09 outage where the proposed method achieves faster stabilisation with reduced transient oscillations and reflects improved recovery dynamics. Figure 13 presents the G03 outage frequency response. The obtained allocation produces the smoothest response and the quickest settling which indicates superior transient behaviour even under less severe disturbances.

The observed performance is consistent with the optimized allocation reported in Table 9, where higher BESS capacities are assigned to electrically influential buses. The results indicate that the PSO-

based solution, together with the proposed power flow informed formulation, improves both frequency indices (nadir and RoCoF) and overall transient frequency behaviour under contingencies of varying severity.

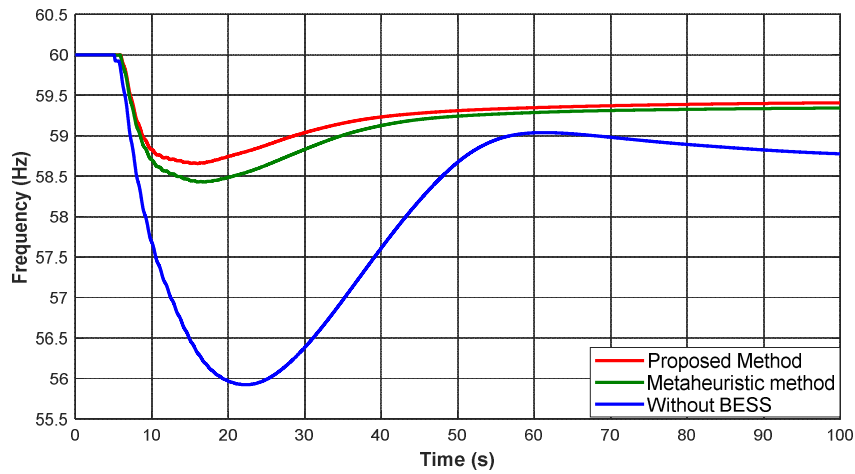


Figure 11. G01 Outage frequency response.

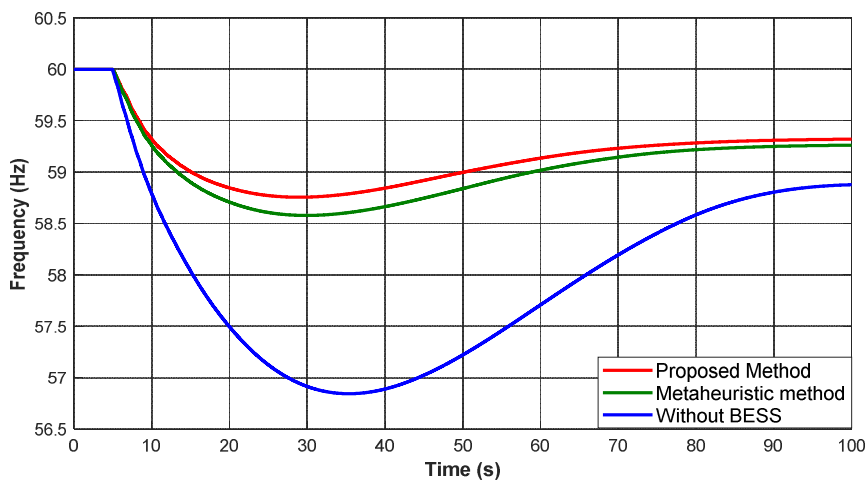


Figure 12. G09 Outage frequency response.

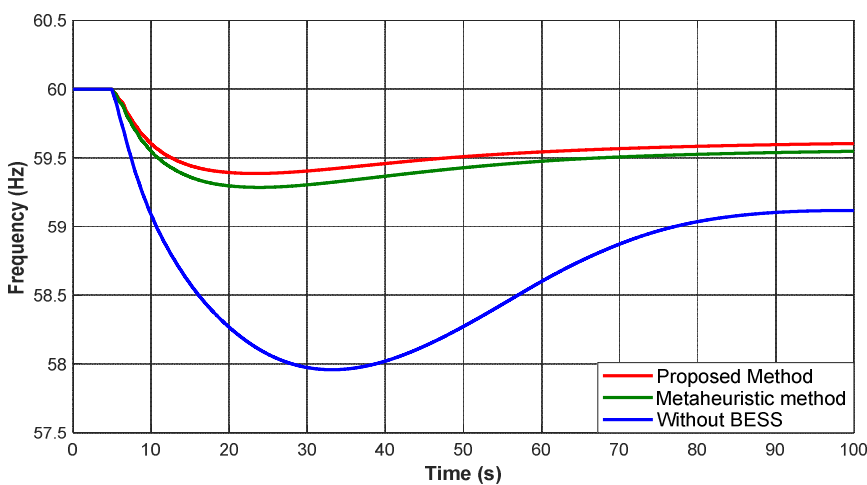


Figure 13. G03 Outage frequency response.

3.9. Impact of Load Decrease Scenario

Section 3.8 demonstrated that the obtained allocation performs effectively under nominal operating conditions. The robustness of this placement is therefore evaluated under a 5% load decrease using the same contingencies. The corresponding frequency indices are reported in Table 11.

Table 11. Frequency stability under load decrease.

Method	G01 Outage		G09 Outage		G03 Outage	
	f_{nadir} (Hz)	RoCoF (Hz/s)	f_{nadir} (Hz)	RoCoF (Hz/s)	f_{nadir} (Hz)	RoCoF (Hz/s)
Proposed Method	58.2983	0.1438	58.6732	0.0538	59.3643	0.0342
Metaheuristic	58.1935	0.1524	58.5421	0.0579	59.2932	0.0378
Without BESS	56.2204	0.2793	57.0305	0.1091	57.9674	0.0773

Figure 14 presents the G01 outage response, where the proposed method exhibits the flattest transient profile and fastest stabilisation, while the baseline case shows a steeper decline and slower recovery. Figure 15 presents the G09 response, where the proposed method achieves smoother recovery with reduced oscillatory behaviour compared to the other methods. Figure 16 presents the G03 response, where the proposed method yields the smoothest response and quickest settling, even under mild disturbance conditions.

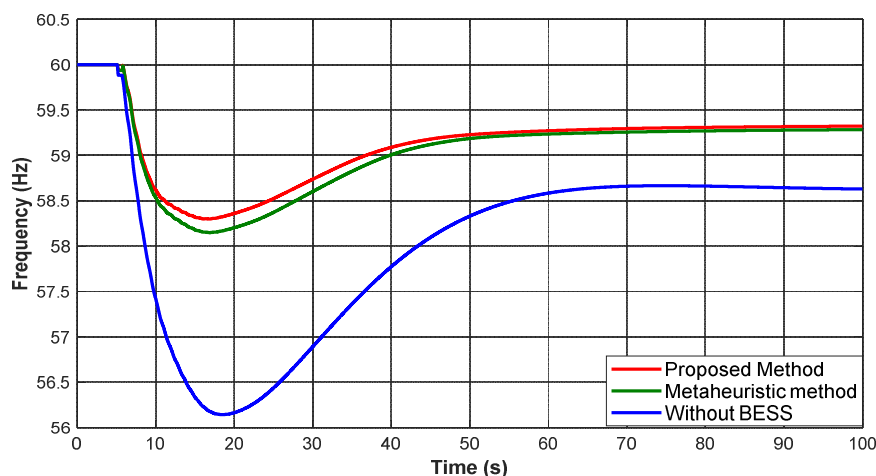


Figure 14. G01 outage under load decrease.

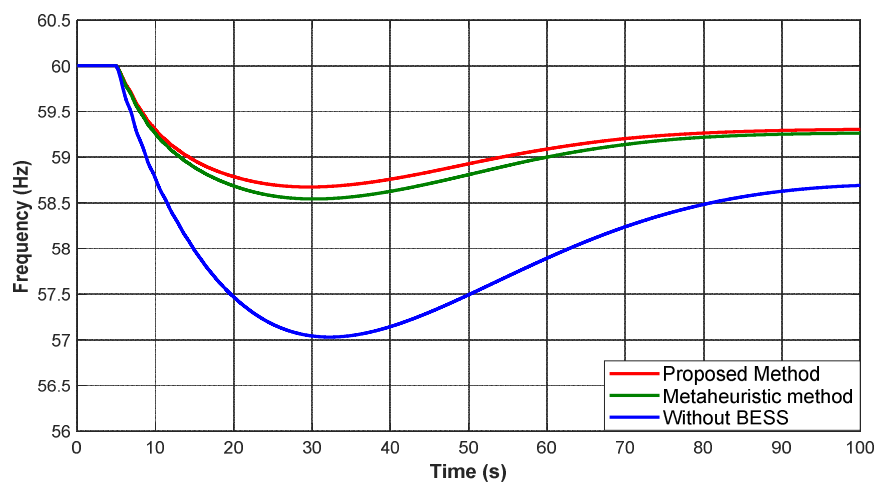
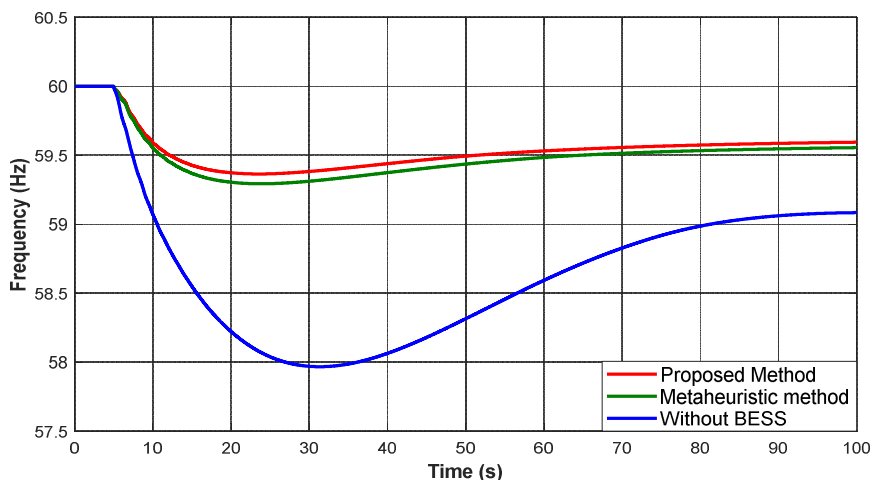


Figure 15. G09 outage under load decrease.**Figure 16.** G03 outage under load decrease.

The trends in Table 11 and the frequency responses confirm that the proposed allocation maintains superior dynamic behaviour under reduced loading, demonstrating robustness to operating point variation.

3.10. Impact of Load Increase Scenario

Following the robustness assessment under reduced loading in Section 3.9, the allocation is further evaluated under a 5% load increase to represent stressed operating conditions. The corresponding frequency indices are reported in Table 12.

Table 12. Frequency stability under load increase.

Method	G01 Outage		G09 Outage		G03 Outage	
	f_{nadir} (Hz)	RoCoF (Hz/s)	f_{nadir} (Hz)	RoCoF (Hz/s)	f_{nadir} (Hz)	RoCoF (Hz/s)
Proposed Method	56.7043	0.1943	57.2366	0.0926	58.2813	0.0622
Metaheuristic	56.0187	0.2093	56.7194	0.1004	57.8106	0.0675
Without BESS	-	-	-	-	55.9587	0.1266

Figure 17 presents the G01 outage response under increased loading. The baseline case exhibits severe degradation in transient behaviour, while the proposed method maintains a smoother profile and faster stabilisation than the metaheuristic method. Figure 18 presents the G09 response, where deeper deviations are observed for all methods. However, the proposed method retains superior containment and recovery characteristics. Figure 19 presents the G03 response, where the proposed allocation again produces the smoothest response and fastest settling.

The performance in Table 12 and the frequency responses indicate that increased loading amplifies frequency stress; however, the proposed method remains effective under these more demanding conditions. The inability of the baseline case to achieve acceptable recovery in some contingencies further highlights the importance of BESS integration under stressed operating points.

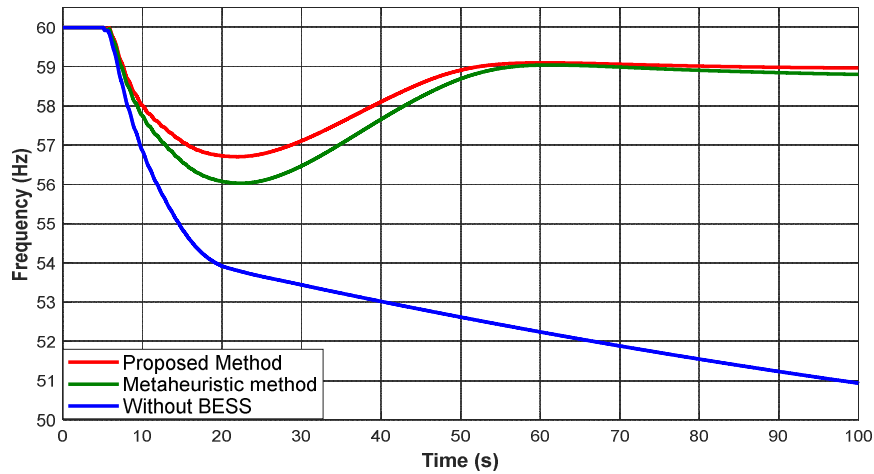


Figure 17. G01 outage under load increase.

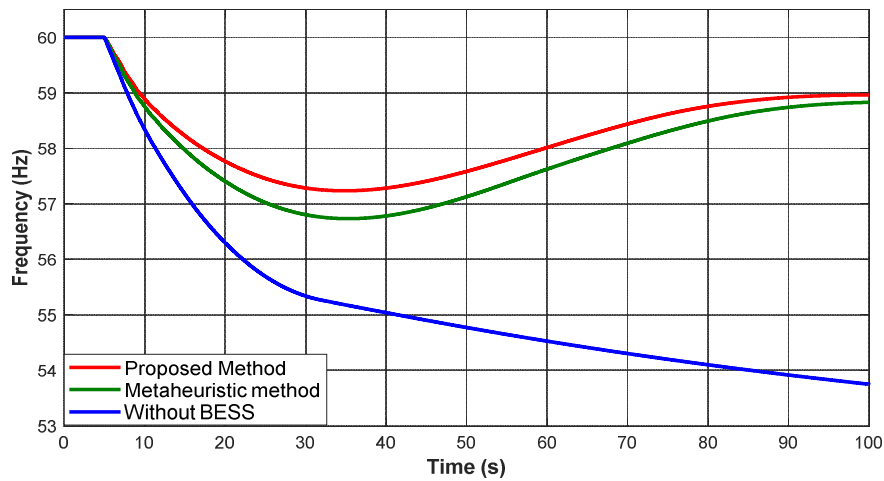


Figure 18. G09 outage under load increase.

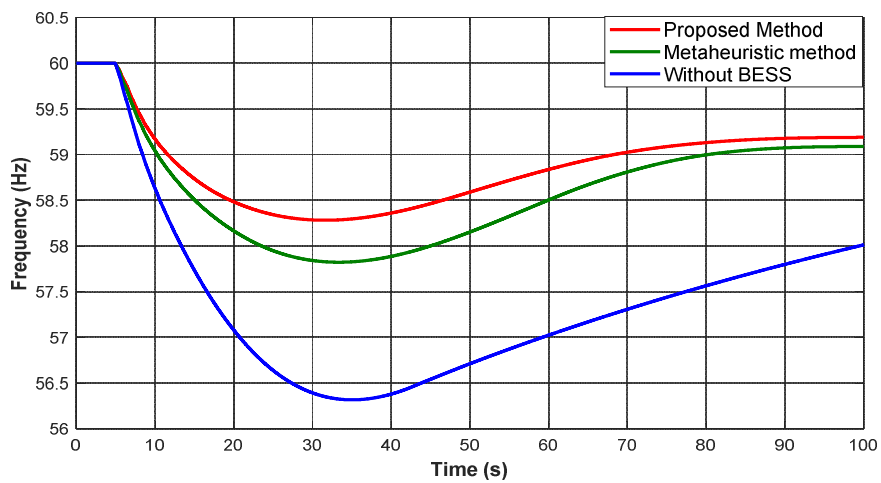


Figure 19. G03 outage under load increase.

3.11. Renewable Energy Integration Scenario

Following the load variation assessments presented in Sections 3.9 and 3.10, the robustness of the obtained BESS allocation is further evaluated under reduced system inertia conditions. To evaluate the impact of renewable energy sources (RES) on frequency stability, the synchronous generating unit G08, rated at 540 MW and connected to Bus 2, was replaced with an equivalent-capacity doubly fed induction generator (DFIG)-based wind generation unit. The replacement was implemented using the standard DFIG model available in DiGSILENT PowerFactory within the RMS dynamic simulation framework. The corresponding frequency stability indices under reduced inertia operation are summarised in Table 13.

Table 13. Frequency stability with wind integration.

Method	G01 Outage		G09 Outage		G03 Outage	
	f_{nadir} (Hz)	RoCoF (Hz/s)	f_{nadir} (Hz)	RoCoF (Hz/s)	f_{nadir} (Hz)	RoCoF (Hz/s)
Proposed Method	58.0275	0.1306	58.3296	0.0574	59.2946	0.0353
Metaheuristic	57.7677	0.1402	58.1223	0.0637	59.1749	0.0374
Without BESS	55.0461	0.2875	56.2756	0.1218	57.3814	0.0877

Figure 20 illustrates the frequency response for G01 outage under wind integration. The baseline case shows a severe frequency decline with a nadir of 55.0461 Hz and a RoCoF of 0.2875 Hz/s which indicates high vulnerability under low inertia conditions. The obtained allocation improves the nadir to 58.0275 Hz and limits the RoCoF to 0.1306 Hz/s which demonstrates effective compensation for the loss of synchronous inertia. Figure 21 presents the G09 outage frequency response. Without BESS support, the system reaches a nadir of 56.2756 Hz. With the obtained allocation, the minimum frequency improves to 58.3296 Hz and the RoCoF is reduced from 0.1218 Hz/s to 0.0574 Hz/s which indicates enhanced disturbance containment under reduced inertia. Figure 22 presents the G03 outage frequency response. The obtained allocation achieves a nadir of 59.2946 Hz compared with 57.3814 Hz without BESS. The associated RoCoF is reduced from 0.0877 Hz/s to 0.0353 Hz/s which confirms improved dynamic performance even under less severe contingencies.

The frequency indices reported in Table 13 confirm that wind integration increases frequency stress in the absence of BESS. In contrast, the obtained allocation consistently mitigates the impact of reduced inertia. The results demonstrate that the proposed allocation remains effective under low-inertia operating conditions, which is essential for future systems with high renewable penetration.

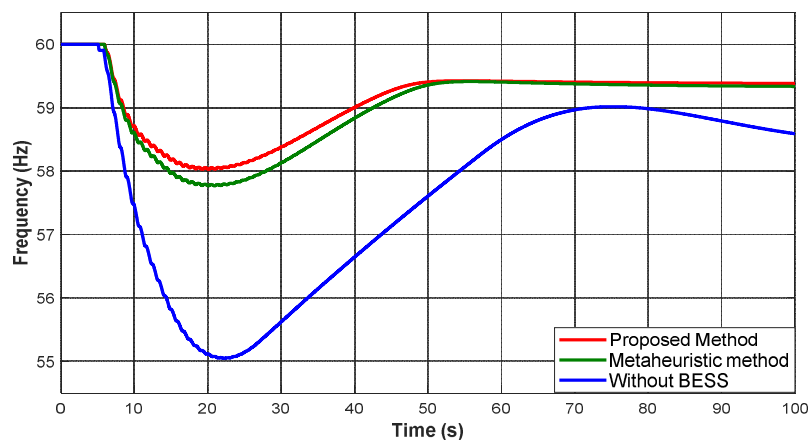


Figure 20. G01 outage with wind integration.

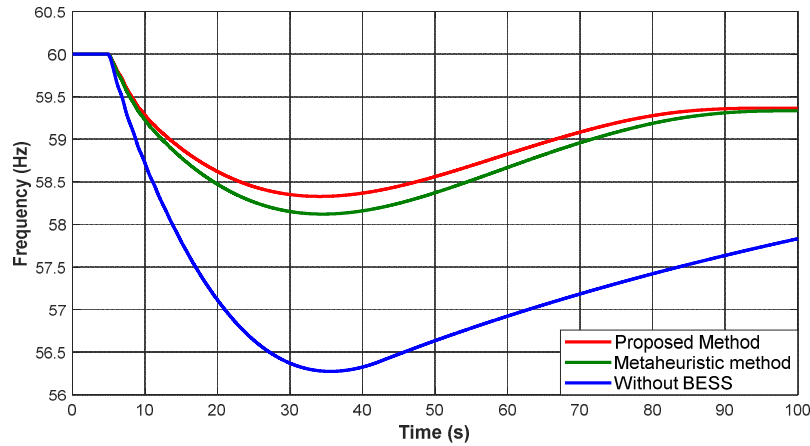


Figure 21. G09 outage with wind integration.

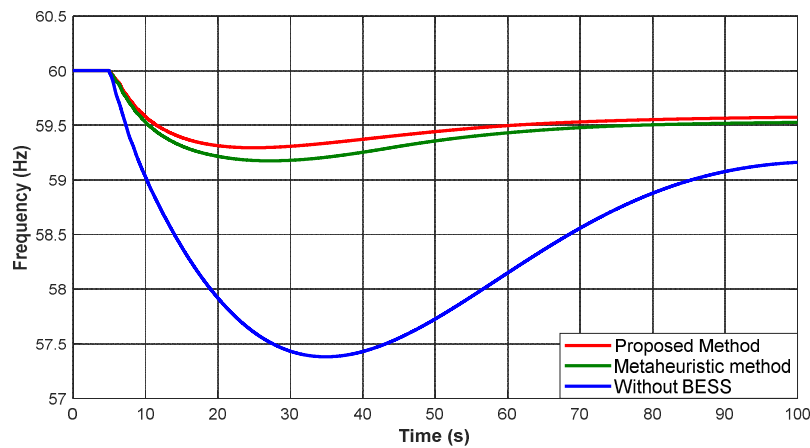


Figure 22. G03 outage with wind integration.

4. Conclusions

This paper presented a power flow informed sensitivity-based method for the optimal placement and sizing of distributed battery energy storage systems (BESSs) to improve frequency stability in low-inertia power systems. The method integrates marginal frequency sensitivity obtained from time domain screening simulations with network coupling information derived from Power flow sensitivities. This integration enables a unified formulation that accounts for both dynamic frequency response and power transfer characteristics of the network.

The application of the proposed optimal placement and sizing method to the IEEE 39-bus New England test system illustrated that BESS locations exhibit non-uniform and nonlinear contributions to frequency nadir and RoCoF improvement. The dynamic simulation results demonstrated that increasing BESS capacity yields diminishing marginal frequency benefits at many buses. The power flow-based analysis further indicated that buses with high marginal frequency sensitivity do not necessarily provide effective network-wide frequency support. This is due to differences in electrical coupling across the network.

The optimization results confirmed that the proposed formulation distributes BESS capacity across multiple buses instead of concentrating capacity at a single location. This allocation reflects the combined influence of marginal frequency contribution and network coupling. Across all considered generator outage contingencies, the proposed method achieved higher frequency nadirs and lower RoCoF values than both the baseline case and the benchmark metaheuristic placement method.

Simulation results under load variation scenarios showed that the proposed placement strategy maintains consistent performance under both reduced and increased loading conditions. Under

increased loading, the proposed method limited frequency deviations more effectively than the comparison methods. In the renewable energy integration scenario, where synchronous generation was replaced by wind generation, the proposed strategy compensated for the reduction in system inertia and maintained acceptable frequency responses across all outages. The proposed method improved frequency nadir by up to 2.7 Hz and reduced RoCoF by approximately 49% compared with the baseline case. These improvements confirm the effectiveness of combining dynamic sensitivity and network coupling information for distributed BESS placement in low-inertia systems.

The proposed method provides a practical approach for enhancing frequency stability in low-inertia power systems using distributed BESSs. The methodology can be extended to larger networks and to formulations that jointly consider frequency and voltage support.

Author Contributions: Conceptualization, L.N. and J.M.; methodology, L.N.; software, L.N.; validation, L.N., J.M., and Y.H.; formal analysis, L.N.; investigation, L.N.; resources, J.M. and Y.H.; data curation, L.N.; writing—original draft preparation, L.N.; writing—review and editing, J.M. and Y.H.; visualization, L.N.; supervision, J.M. and Y.H. All authors have read and agreed to the published version of the manuscript.

Data Availability Statement: The data used in this study are available from the corresponding author upon request.

Abbreviations

The following abbreviations are used in this manuscript:

BESS	Battery Energy Storage System
COI	Centre of Inertia
DIgSILENT	DIgSILENT PowerFactory
MW	Megawatt
PF	Power Flow
PSO	Particle Swarm Optimization
PQ	Active and Reactive Power
PWM	Pulse Width Modulation
RMS	Root Mean Square
RoCoF	Rate of Change of Frequency
SoC	State of Charge

Appendix A

Table A1. BESS Converter and Current Controller Parameters.

Description	Parameter	Value	Unit
Active power filter time constant	T_r	0.01	s
Reactive power filter time constant	T_{rq}	0.1	s
Proportional gain (d-axis current PI controller)	T_p	2	p.u.
Integrator time constant (d-axis current loop)	T_{ip}	0.2	s
Deadband for proportional gain	AC Deadband	0	p.u.
Proportional gain (q-axis current PI controller)	K_q	1	p.u.
Integrator time constant (q-axis current loop)	T_{iq}	0.002	s
Minimum discharging current	id_{min}	-1	p.u.
Maximum charging current	id_{max}	1	p.u.
Minimum reactive current	iq_{min}	-1	p.u.
Maximum reactive current	iq_{max}	1	p.u.

Table A2. Battery Energy Storage Parameters.

Description	Parameter	Value	Unit
Battery energy capacity	C_{bat}	50	MWh
Minimum state of charge	SoC_{min}	0	%
Maximum state of charge	SoC_{max}	100	%
Initial state of charge	$SoC_{initial}$	95	%

Table A3. Frequency Controller Parameters.

Description	Parameter	Value	Unit
Droop coefficient (full active power within $\pm 1-2$ Hz deviation)	Droop	0.004	p.u.
Frequency control deadband	db	0.0004	p.u.

Table A4. Particle Swarm Optimization Parameters.

Description	Parameter	Value
Number of particles	n	40
Number of generations	N_gen	50
Cognitive learning factor	k	0.2
Social learning factor	β	0.5
Inertia weight	ω	0.5

References

1. Das, C.K., et al., Optimal placement of distributed energy storage systems in distribution networks using artificial bee colony algorithm. *Applied energy*, 2018. **232**: p. 212-228.
2. Das, C.K., et al., Optimal allocation of distributed energy storage systems to improve performance and power quality of distribution networks. *Applied Energy*, 2019. **252**: p. 113468.
3. Parajuli, A., et al. Optimal Sizing and Placement of Battery Energy Storage Systems for Enhancement of Grid Frequency Stability. in 2023 10th IEEE International Conference on Power Systems (ICPS). 2023. IEEE.
4. Das, C.K., et al., An optimal allocation and sizing strategy of distributed energy storage systems to improve performance of distribution networks. *Journal of Energy Storage*, 2019. **26**: p. 100847.
5. Thien, T., et al., Real-world operating strategy and sensitivity analysis of frequency containment reserve provision with battery energy storage systems in the german market. *Journal of energy storage*, 2017. **13**: p. 143-163.
6. Okafor, C.E. and K.A. Folly, Optimal placement of BESS in a power system network for frequency support during contingency. *Energy reports*, 2023. **10**: p. 3681-3695.
7. Jani, V. and H. Abdi, Optimal allocation of energy storage systems considering wind power uncertainty. *Journal of Energy Storage*, 2018. **20**: p. 244-253.
8. Baniyadi, A., et al., Optimal sizing design and operation of electrical and thermal energy storage systems in smart buildings. *Journal of Energy Storage*, 2020. **28**: p. 101186.
9. Lian, B., et al., Optimizing LiFePO₄ battery energy storage systems for frequency response in the UK system. *IEEE Transactions on Sustainable Energy*, 2016. **8**(1): p. 385-394.
10. Alhejaj, S.M. and F.M. Gonzalez-Longatt. Impact of inertia emulation control of grid-scale BESS on power system frequency response. in 2016 International Conference for Students on Applied Engineering (ICSAE). 2016. IEEE.
11. Njoka, G.M., L. Mogaka, and A. Wangai, Enhancing grid stability and resilience through BESS optimal placement and sizing in VRES-dominated systems. *Energy Reports*, 2025. **13**: p. 1764-1779.
12. Abayateye, J., et al., BESS Primary Frequency Control Strategies for the West Africa Power Pool. *Energies*, 2022. **15**(3): p. 990.
13. Akram, U., et al., Sizing HESS as inertial and primary frequency reserve in low inertia power system. *IET Renewable Power Generation*, 2021. **15**(1): p. 99-113.

14. Amin, M.R., et al., Application of battery energy storage systems for primary frequency control in power systems with high renewable energy penetration. *Energies*, 2021. **14**(5): p. 1379.
15. Apribowo, C.H.B., et al., Optimal sizing and placement of battery energy storage system for maximum variable renewable energy penetration considering demand response flexibility: A case in Lombok power system, Indonesia. *Energy Conversion and Management: X*, 2024. **23**: p. 100620.
16. Assery, S.A., N. Chen, and X.-P. Zhang, Capacity Optimization and Location of BESS-SC Hybrid System for Grid Inertia Support With High Wind Power Penetration. *IEEE Access*, 2025.
17. Unigwe, O., D. Okekunle, and A. Kiprakis, Smart coordination schemes for multiple battery energy storage systems for support in distribution networks with high penetration of photovoltaics. *IET Smart Grid*, 2019. **2**(3): p. 347-354.
18. ALAhmad, A.K., Voltage regulation and power loss mitigation by optimal allocation of energy storage systems in distribution systems considering wind power uncertainty. *Journal of Energy Storage*, 2023. **59**: p. 106467.
19. Conde, A., et al., Frequency improvement in microgrids through Battery Management System control supported by a remedial action scheme. *IEEE Access*, 2022. **10**: p. 8081-8091.
20. Wang, S., et al., Analysis of energy storage demand for peak shaving and frequency regulation of power systems with high penetration of renewable energy. *Energy*, 2023. **267**: p. 126586.
21. Castro, L.M. and D.R. Espinoza-Trejo, Optimal placement of battery energy storage systems with energy time shift strategy in power networks with high penetration of photovoltaic plants. *Sustainable Energy, Grids and Networks*, 2023. **35**: p. 101093.
22. Ghatuari, I., Controller design and optimal sizing of battery energy storage system for frequency regulation in a multi machine power system. *Energy Reports*, 2024. **12**: p. 4757-4776.
23. Giannitrapani, A., et al., Optimal allocation of energy storage systems for voltage control in LV distribution networks. *IEEE Transactions on Smart Grid*, 2016. **8**(6): p. 2859-2870.
24. Atwa, Y.M. and E. El-Saadany, *Optimal allocation of ESS in distribution systems with a high penetration of wind energy*. *IEEE Transactions on Power Systems*, 2010. **25**(4): p. 1815-1822.
25. Gonzalez-Sanchez, J.W., et al., Optimal Location and Sizing of BESS Systems with Inertia Emulation to Improve Frequency Stability in Low-Inertia Electrical Systems. *Energies*, 2025. **18**(24): p. 6552.
26. Jannesar, M.R., S. Sadr, and M. Savaghebi, Optimal siting, sizing and control of battery energy storage to enhance dynamic stability of low-inertia grids. *IET Renewable Power Generation*, 2024. **18**(15): p. 2925-2941.
27. Ruan, P., et al., Optimal Siting and Sizing of Hybrid Energy Storage Systems in High-Penetration Renewable Energy Systems. *Energies*, 2025. **18**(9): p. 2196.
28. Lee, J., S. Han, and D. Lee, Optimizing the location of frequency regulation energy storage systems for improved frequency stability. *Batteries*, 2023. **9**(12): p. 592.
29. Parajuli, A., S. Gurung, and K. Chapagain, Optimal placement and sizing of battery energy storage systems for improvement of system frequency stability. *Electricity*, 2024. **5**(3): p. 662-683.
30. PowerFactory, D., *Bus new england system*. *Heinrich-Hertz-Str.* **9**: p. 72810.

Disclaimer/Publisher's Note: The statements, opinions and data contained in all publications are solely those of the individual author(s) and contributor(s) and not of MDPI and/or the editor(s). MDPI and/or the editor(s) disclaim responsibility for any injury to people or property resulting from any ideas, methods, instructions or products referred to in the content.